ELSEVIER

NeuroImage

www.elsevier.com/locate/ynimg
NeuroImage 39 (2008) 1 – 9

Diffusion tensor spectroscopy and imaging of the arcuate fasciculus

Jaymin Upadhyay,[a,b] Kevin Hallock,[a] Mathieu Ducros,[a] Dae-Shik Kim,[a] and Itamar Ronen[a,*]

[a] *Department of Anatomy and Neurobiology, Center for Biomedical Imaging, Boston University, School of Medicine, 715 Albany St. X-B01, Boston, MA 02118, USA*
[b] *Program in Neuroscience, Boston University, 5 Cummington St., Boston, MA, USA*

Received 29 March 2007; revised 20 July 2007; accepted 1 August 2007
Available online 7 September 2007

The arcuate fasciculus (AF) is a fiber pathway in the human brain relevant for language processes and has recently been characterized by means of diffusion tensor tractography. The observations made concerning the left and right hemisphere AF include a characterization of the trajectories and quantification of physical properties such as fractional anisotropy, DTI-based fiber density and volume. However, these observations were based on the diffusion of water, which is not particular to either the intra- or extra-axonal compartments, and thus its usefulness for tissue characterization is limited. If the diffusion properties and in turn the geometric properties of only one tissue compartment can be isolated and characterized, a better microstructural characterization of AF is possible. In this study, water-based diffusion tensor probabilistic mapping was first implemented to segment the AF. Subsequently, diffusion tensor spectroscopic measurements of *N*-acetyl aspartate (NAA) were performed to measure the intra-axonal specific diffusion in left and right AF. Diffusion properties of NAA, which solely reflect the intra-axonal space, indicated possible leftward asymmetry in axonal diameter, where those of water, which are not compartment-specific, showed laterality to a lesser extent.

Introduction

Nearly 40 years ago, Geschwind and Levitsky (1968) reported leftward hemispheric lateralization of micro- and macroscopic properties in brain structures relevant to language processing. Since then, numerous groups have found leftward asymmetries (quantities in the left cerebral hemisphere that are greater than in the right cerebral hemisphere) in the gross morphology and cytoarchitecture in brain structures such as the planum temporale (Foundas et al., 1995; Galaburda et al., 1978a,b; Josse et al., 2003; Josse and Tzourio-Mazoyer, 2004; Moffat et al., 1998; Penhune et al., 1996), as well as in more anterior and posterior regions within the temporal cortex (Falzi et al., 1982; Galuske et al., 2000). The leftward asymmetries observed in temporal, parietal or frontal cortices, whether at the microscopic or macroscopic level, have been associated with proper production and comprehension of human language.

With the recent advent of diffusion tensor tractography and probabilistic mapping, a great deal of attention has been given to mapping various short and long range white matter pathways in the human brain (Behrens et al., 2003; Conturo et al., 1999; Jones et al., 1999; Mori et al., 1999; Parker et al., 2003). Due to the fact that traditional human postmortem axonal tract tracing methods, such as injection of DiI (1,1′-dioctadecyl-3,3,3′,3′-tetramethylindocarbocyanine perchlorate), can only define axonal lengths on the scale of tens of millimeters (Galuske et al., 2000; Lukas et al., 1998), diffusion tensor imaging techniques have been particularly valuable in identifying long range axonal projections. In regards to long range pathways relevant to language processing, the arcuate fasciculus (AF) in the left and right hemispheres have been identified in multiple diffusion tensor imaging (DTI) studies (Catani et al., 2005; Makris et al., 2005; Nucifora et al., 2005; Parker et al., 2005; Powell et al., 2006; Vernooij et al., 2007). The AF projects between Wernicke's area (posterior superior temporal gyrus (PSTG) on the Sylvian fissure) and Broca's Area (opercular and triangular regions of the left inferior frontal gyrus). One study by Makris et al. (2005), also examined fractional anisotropy (FA), which has been shown to be related to anisotropic tissue microstructure. FA differences between left and right AF were not particularly significant either within single subject or in group-averaged results. Other studies quantified DTI-based fiber density for both fascicules the AF from neighboring asymmetries (Nucifora et al., 2005; Vernooij et al., 2007). The fiber trajectories from these studies are in good agreement with each other and also with the earliest anatomical work by Dejerine, where a general anatomical description of the AF was given (Dejerine, 1895). These works pave the way towards in-vivo characterization of the AF, but what is still lacking is a more specific description of the differences between left and right AF histological properties such as mean axonal diameter or average myelination.

Conventional DTI provides biophysical measures of axonal bundles, based on the properties of water molecule mobility. In white matter, water diffusion occurs in both intra- and extra-axonal

* Corresponding author. Fax: +1 617 414 2371.
E-mail address: itamar@bu.edu (I. Ronen).
Available online on ScienceDirect (www.sciencedirect.com).

1053-8119/$ - see front matter © 2007 Elsevier Inc. All rights reserved.
doi:10.1016/j.neuroimage.2007.08.046

compartments, and thus an accurate evaluation of axonal features based on diffusion anisotropy is not feasible. Furthermore, histological studies in postmortem human brains that characterize axonal properties of long range white matter pathways are uncommon. Histological work that has defined axonal properties within the AF has not been carried out due to the inability to segment the AF from neighboring fascicules. Thus, as a result of the non-specificity of water diffusion and the unknown fiber composition of the AF, detailed description of fiber composition within the left and right AF is unavailable. Thus, there is great impetus to devise a method that directly details the white matter microstructural properties, and apply it for the description of human AF as well as other fascicules in the brain.

N-acetyl-aspartate (NAA) is a neurometabolite confined to the intra-axonal space in high concentration relative to other metabolites (~10 mM), and thus its diffusion can be used to probe intra-axonal geometric properties (Burri et al., 1990; Nadler and Cooper, 1972; Urenjak et al., 1993). Past studies have measured the diffusion properties of NAA in humans (Ellegood et al., 2005a, b; Harada et al., 2002; Kroenke et al., 2004; Nicolay et al., 2001; Posse et al., 1993). In these studies, the motivation of measuring the diffusion properties of NAA stemmed from the fact that NAA is confined to the intra-neuronal space, and thus its diffusion properties are more closely related to the intracellular geometry. In the study reported here, the diffusion tensor for NAA is measured in both AF as a means to investigate their intra-axonal structure. First, diffusion tensor probabilistic mapping was performed to segment the left and right AF from neighboring fascicules. Once the locations of the left and right AF were identifiable on T_1-weighted anatomical images, diffusion tensor spectroscopic measurements of NAA and water were made in both fascicules to relate the diffusion properties of the intra-axonal space (NAA diffusion) with the diffusion properties of the combined intra- and extra-axonal space (water diffusion).

The DTS measurements of NAA presented here indicate significant differences in the diffusion occurring perpendicular to the principal axonal axis (radial diffusivity) between the left and right AF. Similar trends in water DTS measurements of radial diffusivity from the same volumes of interest (VOIs) were observed but were not significant. This possibly suggests that an intra-axonal difference exists between the two fascicules. The combination of diffusion tensor probabilistic mapping and DTS may provide a new method for characterizing fiber composition of long range white matter pathways.

Methods

Approval for this study was obtained from the Institutional Review Board of Boston University School of Medicine. DTI and DTS data were collected from four healthy right-handed male subjects (32.25±8.5 years). Informed consent from each volunteer was obtained prior to the session. DTI, DTS and T_1-weighted structural imaging were all performed on a 3-T Philips Intera scanner (Philips Medical Systems, Cleveland, Ohio) with 2.2 G/cm maximum gradient strength. DTI data and the first set of T_1-weighted images were collected using a six-channel SENSE receiver coil, while DTS measurements and the T_1-weighted images necessary for spectroscopic voxel placement were collected using a quadrature Transmit/Receive head coil. The SENSE receiver coil was used to reduce the acquisition time for DTI data collection.

Diffusion tensor imaging and probabilistic mapping

DTI and T_1-weighted anatomical images were acquired to segment and identify the left and right AF in each subject. DTI: pulse sequence = single shot SE-EPI, TR/TE = 10646/91 ms, *b*-value = 1000 s/mm^2, FOV = 230 × 230 mm^2, resolutions = 1.8 × 1.8 × 2.0 mm^3, number of diffusion directions = 15, 73 axial slices. T_1-weighted images: pulse sequence = 3D MP-RAGE, TR/TE = 7.47 ms/3.4 ms, flip angle = 8.0°, FOV = 230 × 230 mm^2, resolution = 0.9 × 0.9 × 1.0 mm^3, 160 axial slices. Three DTI data sets were acquired, corrected for motion, coregistered and averaged within and between acquisitions. Single subject DTI and diffusion tensor probabilistic mapping analyses were performed using an in-house MATLAB-based software package (Mathworks Inc. Natick, MA) (Lehericy et al., 2004). DTI and anatomical data sets were first manually coregistered using the (1) corpus callosum, (2) the lateral ventricles, (3) the left and right sylvian fissures and (4) the left and right lateral sulci as landmarks. Regions of interests (ROI) defining the posterior superior temporal gyrus (PSTG) and pars opercularis (posterior Broca's area) were identified on the coregistered T_1-weighted data set in both cerebral hemispheres and used for ROI constrained probabilistic mapping. The use of a 3D anatomical atlas aided the identification of the pars opercularis and PSTG for each subject (Duvernoy, 1999). The pars triangularis portion of Broca's area was avoided when defining the inferior prefrontal cortex ROI to prevent inclusion of 'u' fibers projecting between the pars opercularis and triangularis that are not part of the AF. The pars opercularis was defined on axial slices as the region bordered anteriorly by the vertical ramus of the lateral fissure and pars triangularis, while in the posterior direction the pars opercularis was bordered by the precentral gyrus and inferior precentral sulcus. The PSTG or Wernicke's area was defined as the region on planum temporale (Gannon et al., 1998; Hopkins et al., 1998) bordered posteriorly by the angular gyrus and ascending posterior segment of the superior temporal sulcus, while being bordered by the supramarginal gyrus in the superior direction. For both the pars opercularis and PSTG, ROIs were extended to approximately 4–5 mm of surrounding white matter. ROI constrained probabilistic mapping was achieved with the probabilistic mapping method initially proposed by Parker et al. (2003) and has also been described in detail in our recent work (Upadhyay et al., 2006).

Diffusion tensor spectroscopy

DTS was subsequently performed in separate scanning sessions in the left and right AF. Using probabilistic maps of the left and right AF superimposed on T_1-wieghted images, spectroscopic volumes of interests (VOI = 4.0 × 1.0 × 1.0 cm^3) were positioned on sagittal, coronal and axial T_1-weighted images acquired just prior to the DTS measurements. The spectroscopic volume included only the section of the AF running primarily in the anterior–posterior direction (Fig. 1). Posterior segments of the AF, referred to as the vertical segments of the AF by Makris et al. (2005), projecting to the very lateral PSTG and anterior segments projecting to lateral pars opercularis were excluded from the VOI. Inclusion of nearby gray matter and white matter of other fascicules were minimized in the spectroscopic VOI, by angulating and positioning the VOI along the AF. Single voxel NAA and water diffusion measurements were obtained by incorporating diffusion gradients within a standard point-resolved

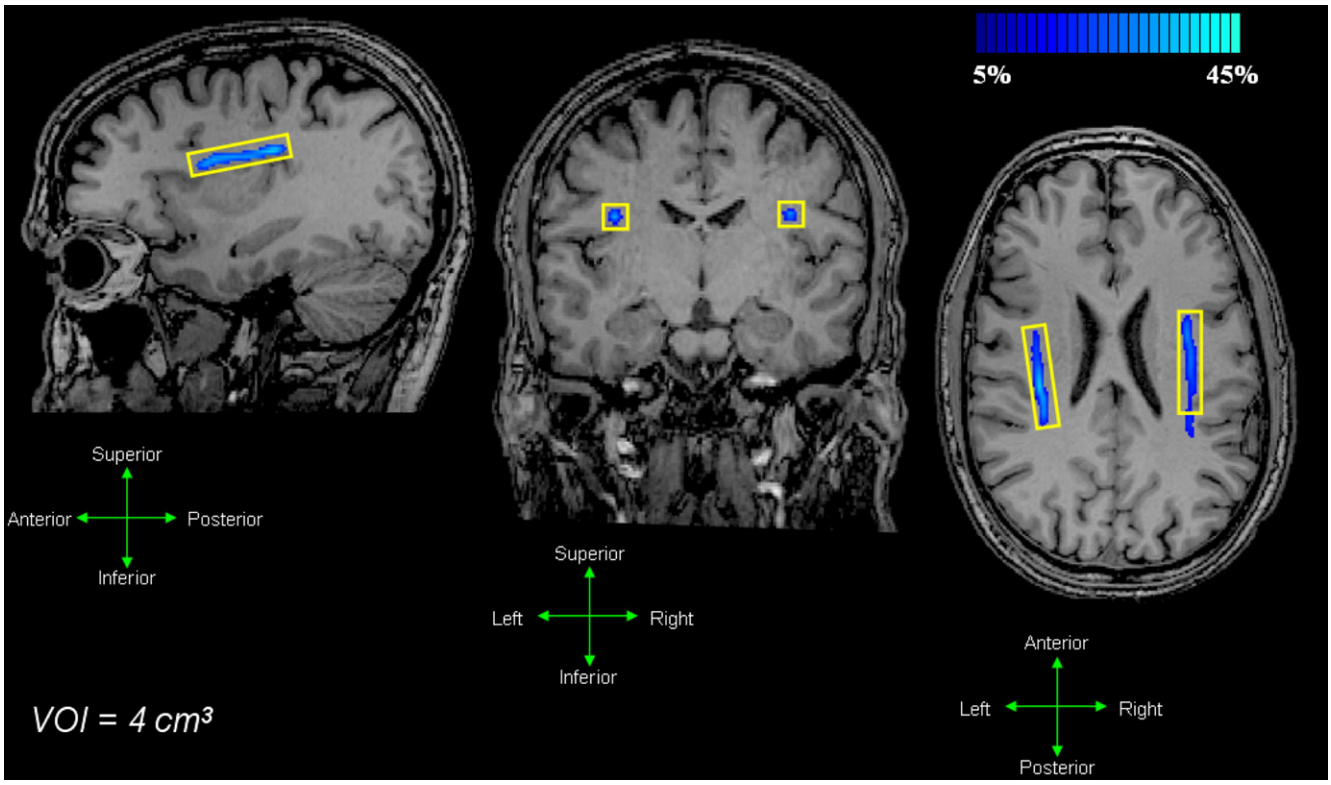

Fig. 1. 2D diffusion tensor probabilistic maps of the left and right arcuate fasciculus. Probabilistic mapping showed a slight and insignificant leftward laterality in probability or fiber density (Table 1). Areas of the AFs depicted in light blue-green have a higher percentage (~45%) of fibers that go through a given voxel in comparison to blue voxels which have lower percentage (~10%) of fibers. For each subject, 2D probabilistic maps of the left and right AF in sagittal, coronal and axial planes were used to position the DTS VOI (shown in yellow) during measurement of NAA and water diffusion. In DTS experiments, the VOI ($4.0 \times 1.0 \times 1.0$ cm^3) was positioned over the AF segment running in the anterior–posterior direction.

spectroscopic (PRESS) sequence (minimum TR = 3000 ms, TE = 135 ms). In each VOI, cardiac-gated NAA and water diffusion measurement were made using three distinct *b*-values: (1) 161.02 s/mm^2, (2) 779.38 s/mm^2 and (3) 1648.90 s/mm^2 with g = 0.5, 1.1 and 1.6 G/cm, respectively. At each *b*-value, δ and Δ were kept constant at 30 ms and 60 ms, respectively. For each *b*-value, diffusion weighting was applied in six directions: [1 0 1] [1 1 0] [0 1 1] [0 1 −1] [−1 0 1] [1 −1 0]. 2048 data points per scan were collected with a 3-kHz spectral window. Sixty-four spectra were acquired for NAA diffusion characterization, while only 8 spectra were necessary for water diffusion characterization. Water suppression during NAA diffusion measurements was performed such that a substantial residual water peak was still present, enabling zero-order phase correction to be performed on each of the 64 spectra prior to averaging. Zero-order phase correction was also performed on each of the eight water DTS measurements. Phase correction to individual and averaged NAA and water spectra were performed using in-house MATLAB 7.0 scripts (Mathworks Inc. Natick, MA). Subsequent procedures of (1) baseline offset adjustments, (2) fitting of phase corrected and averaged spectra to Lorentzian line shapes and (3) peak integrations of fitted peaks were performed using OriginLab 7.5 (Origin Lab, Northampton, MA).

Peak integrals of the fitted NAA and water spectra for each *b*-value and each of the six diffusion directions were measured to yield the respective diffusion tensors. From the diffusion tensors, the trace ADC, FA, radial diffusivity (RD, $(\lambda_2+\lambda_3)/2$) and axial diffusivity (AD, λ_1) were calculated for NAA and water in both AFs. The RD is the diffusion occurring perpendicular to the main fiber axis and is compared to the AD which is the diffusion occurring parallel to the main fiber axis. Lastly, the symmetry coefficient (SC), SC = (L − R)/[0.5(L + R)] for FA, RD and AD were calculated (Galaburda et al., 1987; Makris et al., 2005). A two-way ANOVA test was used for all statistical analysis.

Results

Segmentation of the arcuate fasciculus

Fig. 1 shows the 2D diffusion tensor probabilistic maps of the left and right AF obtained from Subject 4. The segments of the probabilistic maps coded in a light blue-green color represent a high density of fibers, while those coded in blue indicate white matter voxels with a low fiber density. Fig. 2 shows a 3D representation of the left and right AF (shown in white) projecting primarily in the anterior–posterior direction on the diffusion direction encoded images also from Subject 4. In the coronal (Fig. 2A) and sagittal (Fig. 2B) planes, it can be seen that the ROI-constrained probabilistic mapping method enables the AF to be identified, and also differentiated from adjacent fiber pathways such as more dorsal sections of the superior longitudinal fasciculus or superior corona radiata. Figs. 1 and 2 both depict the segments of the AF in which the DTS measurements were performed. In Table 1, probability values of the full length of the left and right AF

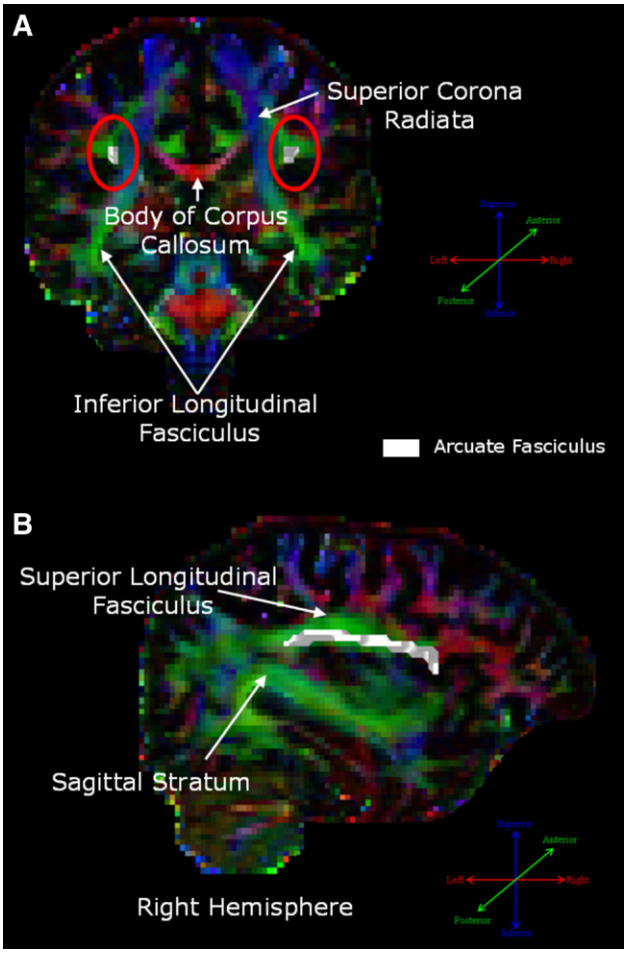

Fig. 2. 3D diffusion tensor probabilistic maps of the left and right arcuate fasciculus. The 3D probabilistic AF bundle (shown in white) is depicted on diffusion direction encoded FA maps in the coronal (A) and sagittal (B) planes. In the diffusion direction encoded maps, the anterior–posterior AF segments are shown and correspond to the location where DTS measurements were made. Panel A depicts a coronal slice positioned close to the posterior segments of the left and right AF. In the sagittal view, the right hemisphere AF spans the distance between the interior prefrontal cortex to the caudal regions of the sylvian fissure (B). The sagittal slice is positioned at the medial edge of the right hemisphere AF and slightly cuts into the AF.

(posterior superior temporal gyrus to pars opercularis) are given for each subject. Here it can be seen that in both the single subject and group-averaged (n=4) probability values between left and right AF do not vary greatly ($p=0.13$). An insignificant ($p=0.08$) difference was observed in DTI-based FA values, where the group-averaged FA in the left and right AF were 0.52 ± 0.01 and 0.45 ± 0.05, respectively.

DTS of the arcuate fasciculus

Fig. 3 shows typical water suppressed DTS spectra obtained with two diffusion weighting values and two different gradient directions. It can be seen that good SNR is maintained even at the higher *b*-value.

The trace apparent diffusion coefficients (ADC) of water as calculated from DTI and non-water suppressed DTS were found to be similar to each other and to those reported in DTI literature (Zhai et al., 2003). Encouragingly, the DTI and DTS ADC values for the left AF were 0.62 ± 0.01 $\mu m^2/ms$ and 0.68 ± 0.07 $\mu m^2/ms$, respectively. In the right AF, the DTI and DTS ADCs were respectively 0.63 ± 0.03 $\mu m^2/ms$ and 0.69 ± 0.08 $\mu m^2/ms$. In contrast, the FA (Water) as determined by DTS was much lower in comparison to DTI (Table 1). DTS measurements showed significantly higher values in the left AF ($p=0.01$).

The trace ADCs of NAA were found to be similar between left and right AF. ADC values for the left and right AF were respectively 0.17 ± 0.01 $\mu m^2/ms$ and 0.18 ± 0.004 $\mu m^2/ms$. The FA(NAA) was significantly greater in the left AF than it was in the right AF ($p=0.01$). The FA values of NAA were always significantly greater than those of water in both left and right AF ($p<0.002$). In Table 1, although the symmetry coefficient (SC) for FA(NAA) was greater than FA(Water), this difference was found to be insignificant ($p=0.52$). Positive SC values correspond to greater magnitudes in the left AF, while negative SC values denote greater magnitudes in the right AF.

The radial and axial diffusivities of NAA and water as measured by DTS were also compared. It was observed that both radial and axial diffusivities between NAA and water in left and right AF always varied significantly ($p=0.001$). The significant difference in RD and AD were expected given that the ADC(NAA) is much smaller than the ADC(Water). The radial diffusivities (RD) of NAA and water were both lower in left AF, but only significantly lower ($p=0.05$) for RD(NAA) (Table 1). Rightward asymmetries of -0.16 and -0.05 were calculated for RD(NAA) and RD(Water), respectively. Conversely, the group-averaged AD(NAA) and AD(Water) was lower in the right AF than in the left (Table 1) with the former being significant ($p=0.02$). Radial and axial diffusivity SC values between NAA and water were also compared. Here it was observed that only the differences in SC values for radial diffusivity were significant ($p=0.02$; F-stat=15.86).

Two-way ANOVA was performed on the water and NAA DTS data where the two factors chosen were hemisphere (L–R) and substance (NAA–H_2O) to also look for interactions. The interactions [substance × hemisphere] were calculated for FA, RD and AD of NAA and H_2O in both hemispheres. The interaction term for FA values yielded $p=0.077$, which is not significant. For the analysis of AD and RD, the two-way ANOVA was performed on AD/ADC and RD/ADC, where ADC is the trace apparent diffusion coefficient of NAA and H_2O. The normalization by the ADC removed the large difference due to the basic diffusivity difference between the two substances (NAA or H_2O) and allowed for a more balanced estimation of the interaction. *P*-values for the interaction [substance × hemisphere] for both RD and AD were highly significant, $p=0.0056$. This is corroborated by the results in Table 1, where both AD and RD of NAA show significant hemispheric dependence, and the AD and RD of water display a much lower dependence on hemisphere.

To further estimate the implication of hemisphere-related changes in DTS parameters of NAA and H_2O, correlation analysis between RD and AD was performed for NAA and water diffusion (Fig. 4). For correlation analysis, RD and AD values from left and right AF were combined. Fig. 4 shows a rather insignificant correlation between RD(NAA) and AD(NAA) ($r=-0.55$, $r^2=0.30$), implying that the changes in RD(NAA) between the two hemispheres were more significant than the changes in AD (NAA). Conversely, a significant correlation between RD(Water) and AD(Water) was also detected ($r=0.93$, $r^2=0.86$). Moreover, a

Table 1
Diffusion properties of NAA and water in left and right arcuate fasciculus

		Sub. 1	Sub. 2	Sub. 3	Sub. 4	Mean	*P*-value	*F*-stat	SC
Probability %	Left	18.64	24.14	19.69	22.14	21.15±2.47	0.13	4.45	0.04
	Right	16.80	23.89	19.38	21.44	20.38±3.01			
FA(Water) DTI	Left	0.53	0.50	0.52	0.52	0.52±0.01	0.08	7.09	0.14
	Right	0.44	0.46	0.40	0.52	0.45±0.05			
FA(Water) DTS	Left	0.26	0.26	0.25	0.26	0.26±0.008	0.01*	36.76	0.18
	Right	0.22	0.20	0.20	0.23	0.21±0.01			
AD(Water) λ_1, $\mu m^2/ms$	Left	0.75	0.91	0.93	0.80	0.85±0.09	0.30	1.56	0.03
	Right	0.70	0.93	0.87	0.80	0.83±0.10			
RD(Water) $(\lambda_2+\lambda_3)/2$, $\mu m^2/ms$	Left	0.52	0.62	0.65	0.56	0.59±0.06	0.18	3.03	−0.05
	Right	0.52	0.70	0.66	0.59	0.62±0.08			
FA (NAA)	Left	0.50	0.54	0.48	0.60	0.53±0.06	0.01*	25.86	0.21
	Right	0.44	0.42	0.40	0.45	0.43±0.02			
AD(NAA) λ_1, $\mu m^2/ms$	Left	0.28	0.26	0.28	0.28	0.27±0.008	0.02*	19.81	0.08
	Right	0.26	0.25	0.25	0.25	0.25±0.005			
RD(NAA) $(\lambda_2+\lambda_3)/2$, $\mu m^2/ms$	Left	0.12	0.11	0.13	0.10	0.12±0.01	0.05*	11.00	−0.16
	Right	0.14	0.14	0.14	0.13	0.14±0.005			

Single subject and group-averaged diffusion properties of NAA and water in left and right AF. Values are given for probability, fractional anisotropy (FA), axial diffusivity (AD) and radial diffusivity (RD). Group-averaged symmetry coefficients (SC) are also give (positive values = left lateralization, negative values = right lateralization); SC = (L − R)/[0.5(L + R)]. Only the differences for radial diffusivity SC values between NAA and water were significant ($p = 0.02$; F-stat = 15.86) F-stat = *F-Statistic and F-Critical* = 10.21. *Indicates significance.

Fisher z-transform analysis showed that the two correlations were statistically different ($Z = 3.60$; Z-critical = 1.96 for $p = 0.05$).

Discussion

This study combined diffusion tensor probabilistic mapping with diffusion tensor spectroscopy to characterize histological properties of AF. Similar to previous works, this study initially utilized DTI to identify and characterize the left and right AF in the human brain (Catani et al., 2005; Makris et al., 2005; Nucifora et al., 2005; Parker et al., 2005; Powell et al., 2006; Vernooij et al., 2007). From the DTI results, we observed left lateralization of quantities such as FA and DTI-based fiber density, in accord with previous DTI studies. The density of the AF bundles showed an insignificant leftward asymmetry in group-averaged results. This is in contrast to previous studies where lateralization in the relative fiber density was found to be significant (Nucifora et al., 2005; Vernooij et al., 2007). A possible reason for the discrepancy can be attributed to the fact that deterministic fiber tracking rather than probabilistic mapping methods were used in the earlier studies. Also, the choice of the seeding ROIs corresponding to Broca's and Wernicke's area can impact the resulting fiber density. As mentioned above, this study omitted the pars triangularis from the Broca's Area ROI to avoid the 'u' fibers within the inferior prefrontal cortex.

This study implemented DTS in both fascicules to characterize diffusion properties specific to the intra-axonal space. As shown in Table 1, the FA values as determined by both DTI and DTS of water and NAA were greater in the left AF, but only significantly greater for DTS measurements. The FA of water calculated from the DTI data were consistently greater than those obtained from DTS-based water measurements. This is not surprising since changes in the main direction of the fiber tract within the DTS volumes will necessarily impact the FA. The comparison of radial diffusivities (RD) of NAA and water best enabled an assessment of the axonal properties in left and right AF. It is important to emphasize the necessity of performing DTS measurements both on NAA and water. Comparing left and right AFs diffusion properties of only NAA provides an incomplete link to tissue microstructural assessment. Macroscopic curvature may affect the assessment of the eigenvalues of the diffusion tensor such that variations between left and right AFs would not be due to changes in e.g. axonal diameter or microscopic organization, but rather due to changes in tract trajectory in the large VOI. The ability to compare the eigenvalues of the diffusion tensor of NAA in both AFs with those of water taken from the same VOIs helps to factor out the effect of macroscopic curvature since the curvature similarly affects the NAA and water diffusion in the intracellular compartment.

A calculation and comparison of RD(NAA) was particularly beneficial given that it is the intra-axonal properties of each axonal bundle that primarily determine the RD(NAA), whereas the RD (Water) is a reflection of the combined intra- and extra-axonal geometries. The RD(NAA) and RD(Water) both increased between the left and right AF; however, the increase was only significant for the radial diffusivity of NAA. The larger increase for RD(NAA) was further confirmed by group-averaged symmetry coefficients (SC), which showed a significantly higher rightward laterality for RD(NAA) in comparison to RD(Water). Moreover, of all comparisons of SC values between NAA and water, only the SC values for RD varied significantly. The axial diffusivities (AD) of NAA and water showed a decrease between left and right AF, where the difference was significant for AD(NAA). Given that the left and right AF do not follow exactly the same trajectory, it is most likely that the macroscopic curvature effects vary between the two fascicules and affect λ_1 differentially.

An important finding of this study was the lack of a strong correlation ($r^2 = 0.30$) between the RD(NAA) and AD(NAA) as depicted in Fig. 4. Changes in macroscopic curvature are expected to result in a significant correlation between radial and axial diffusivities. This result is a good indication that the RD(NAA) is not significantly confounded by factors such as macroscopic curvature of the fiber tract, and the variation in RD(NAA) stems primarily from changes in intra-axonal microstructure between left and right AF. On the other hand, the bottom correlation plot in Fig. 4 shows RD(Water) and AD(Water) to be significantly correlated ($r^2 = 0.86$).

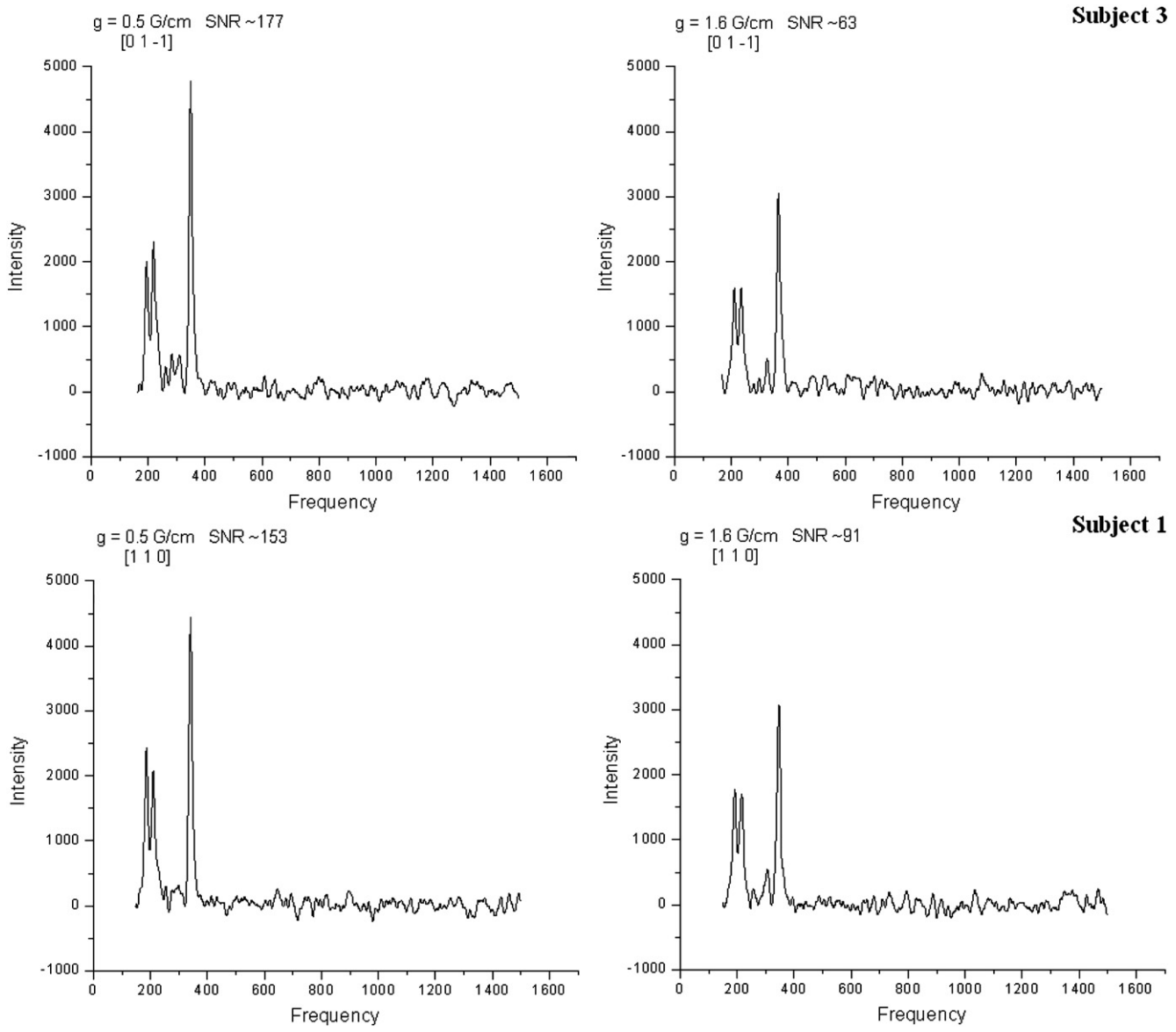

Fig. 3. Diffusion-weighted spectra in left and right arcuate fasciculus. A significant signal attenuation of the NAA signal intensity was detected as the diffusion weighting magnitude was increased. Data are shown from two subjects when diffusion weighting magnitudes of $b=161.02$ s/mm^2 and $b=1648.48$ s/mm^2 were applied in the [0 1 −1] direction (top spectra) and [1 1 0] direction (bottom spectra). Spectra obtained with a diffusion weighting of 779.38 s/mm^2 is not shown. In the top set of spectra, measurements from the left AF are shown for Subject 3, whereas in the bottom spectra diffusion-weighted measurements from the right AF of Subject 1 are shown. Both water-suppressed measurements show more than adequate SNR for characterizing NAA diffusion properties.

The exact causes for this latter correlation were not resolved in this study, but may result from extra-axonal diffusion factors. If the strong correlation is indeed a result of extra-axonal properties such as myelination, further justification is given to the necessity of measuring intra- and extra-axonal diffusion properties separately. The top graph in Fig. 4 also shows a separation of left and right arcuate fasciculus NAA data points as a function of radial diffusivity. This clustering is not seen for the left and right water data points.

Similar to previous DTS studies, this study observed anisotropic intra-axonal diffusion, as defined by compartmentalized NAA diffusion (Ellegood et al., 2006). Axonal diameter is a microstructural property that can predominantly determine the extent to which radial diffusion occurs within the intra-axonal compartment and in turn, the anisotropy of intra-axonal diffusion (Beaulieu and Allen, 1994a,b; Takahashi et al., 2002). Larger axonal diameters can explain the significant differences observed in RD(NAA) between left and right AF. Differences in left and right radial diffusivity of water, on the other hand, can not be unequivocally linked to concomitant differences in axonal diameter between those areas. Water radial diffusivity is affected by axonal density, axonal diameter and degree of myelination, all of which may be different in the two AFs. Song et al. (2002, 2005) robustly linked demyelination to increases in water radial diffusivity as calculated from DTI data. Beaulieu and Allen (1994a) performed in vitro diffusion measurements on three myelinated and unmyelinated fish nerves. This study reported that myelination per se is not a contributing factor to anisotropic diffusion supporting the notion that it is the combination

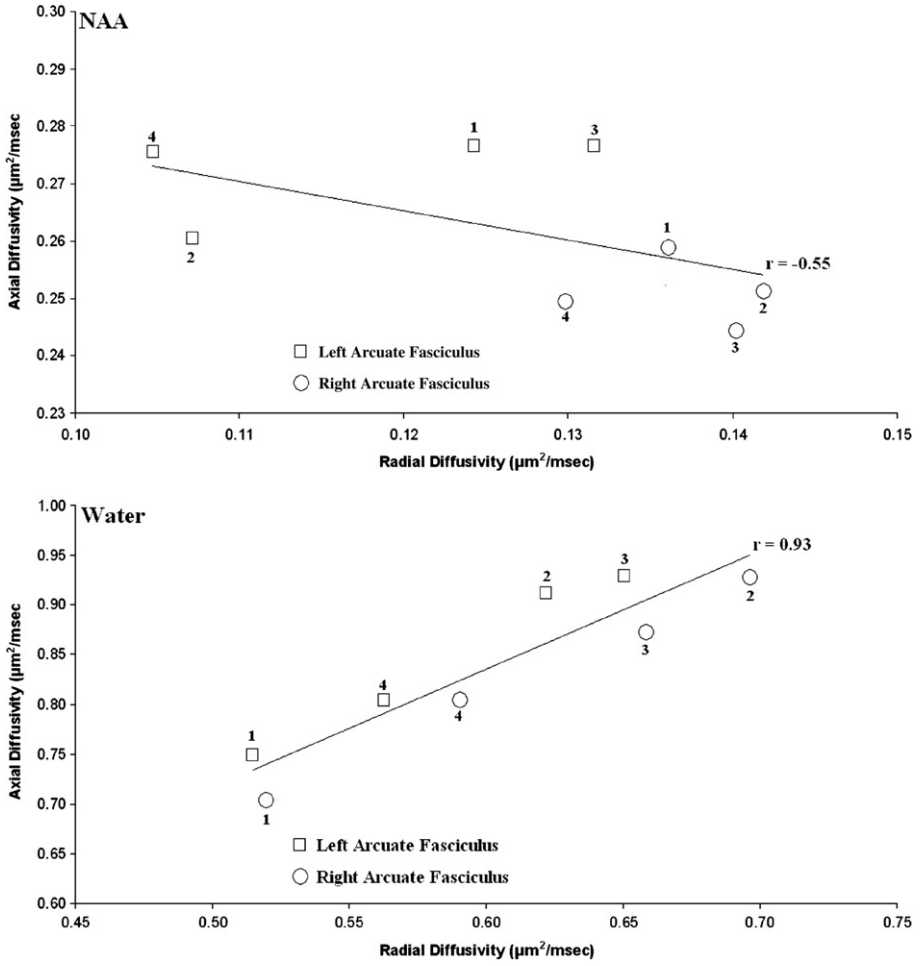

Fig. 4. Correlation between radial diffusivity (RD) and axial diffusivity (AD) of NAA and water. An insignificant correlation between RD(NAA) and AD(NAA) was detected as shown in the top correlation plot. With 6 degrees of freedom, a minimum correlation of ±0.71 would be necessary for significance at $p=0.05$. This lack of a correlation as well as the clustering of the data points further points to a difference in the intra-axonal properties between the left and right AF. Conversely, the correlation between RD(Water) and AD(Water) was significant as shown in the bottom plot. The cause of this strong correlation is not clearly understood. Data points include all AD and RD measurements made in the left and right AF. Numbers above each data point correspond to subject number. The two correlations were found to differ significantly ($Z=3.60$; Z-critical $=1.96$ for $p=0.05$).

of structural factors, rather than just axonal diameter that defines water radial diffusivity and FA.

The authors realize that a previous histological characterization of the AF axonal diameter and/or myelination would have greatly strengthened the results and connections made between intra-axonal NAA diffusion and axonal diameter. Knowing the precise histological properties of left and right AF can contribute to an understanding of how these pathways enable proper function of the areas that they connect. As suggested originally by Lamantia and Rakic (1990) and later by Aboitiz et al. (1992), small diameter corpus callosum axons, such as those found in the genu, which project to prefrontal areas are more suitable for carrying a tonic signal, while large diameter axons of the body which project to motor cortices are necessary to transmit a fast phasic signal. Having this kind of information about the AFs can possibly help elucidate their ability to support a particular function or a given computational demand.

One limitation of the present study was that a differentiation between NAA and NAAG was not made, where the latter is not necessarily specific to the intra-axonal space. Although NAAG is at a much lower concentration in comparison to NAA, a distinction between NAA and NAAG would have made the characterization of intra-axonal diffusion properties more accurate. However, the main constraint of this study arose from the fact that a rather large spectroscopic VOI was implemented in order to obtain sufficient SNR, particularly for diffusion-weighted NAA measurement. Outcomes of this particular limitation include a susceptibility to the macroscopic curvature of AF fibers, which can cause diffusion measures such as FA to be lower than expected. Furthermore, the utilization of a large VOI could also introduce partial volume effects with neighboring white matter tracts, which can introduce error into the measurements. Partial voluming is unavoidable because VOIs necessarily have a rectangular shape. The knowledge of the precise location of the left and right AFs, in conjunction with the ability to angulate the long and narrow VOI ($4.0\times1.0\times1.0$ cm^3) does, however, minimize partial voluming as much as possible (Fig. 1). It was estimated that the group-averaged percentages ± standard deviations of arcuate fasciculus within the left and right DTS VOIs were approximately 85%±5% and 76%±6%, respectively. This difference between the left and right VOIs cannot be excluded a source of error in the estimation of the DTS quantities for both AFs.

Also, it must be noted that these percentages can vary significantly depending on the probability threshold implemented. Although diffusion tensor probabilistic mapping can identify and segment a particular fascicule, it remains difficult to exactly determine all white matter voxels belonging to a specific fascicule.

Conclusion

This study implemented DTI to first segment the left and right AF. We found a leftward asymmetry in FA and fiber density as determined with probabilistic mapping, which is consistent with previous work. Diffusion tensor spectroscopic measurements of NAA were then performed to characterize the intra-axonal diffusion properties in each fasciculus, as well as compare NAA diffusion with the combined intra- and extra-axonal diffusion of water. The correlation results between RD(NAA) and AD(NAA) in conjunction with the tensor properties characterizing NAA and water diffusion suggests that there is a significant difference in intra-axonal properties between the left and right arcuate fascicules, and these differences are possibly linked to differences in average axonal diameters. The combined use of DTI and DTS may be a new method to measure and further characterize microstructure in long range white matter fascicules, providing a more accurate means to relate structure to function in the human brain.

Acknowledgments

This work was supported by NIH Grant NS44825. The authors would like to thank Dr. Francisco Aboitiz for helpful discussion on the arcuate fasciculus.

References

Aboitiz, F., Scheibel, A.B., Fisher, R.S., Zaidel, E., 1992. Fiber composition of the human corpus callosum. Brain Res. 598 (1–2), 143–153.

Beaulieu, C., Allen, P.S., 1994a. Determinants of anisotropic water diffusion in nerves. Magn. Reson. Med. 31 (4), 394–400.

Beaulieu, C., Allen, P.S., 1994b. Water diffusion in the giant axon of the squid: implications for diffusion-weighted MRI of the nervous system. Magn. Reson. Med. 32 (5), 579–583.

Behrens, T.E.J., Johansen-Berg, H., Woolrich, M.W., Smith, S.M., Wheeler-Kingshott, C.A.M., Boulby, P.A., Barker, G.J., Sillery, E.L., Sheehan, K., Cicarelli, O., Thompson, A.J., Brady, J.M., Matthews, P.M., 2003. Noninvasive mapping of connections between human thalamus and cortex using diffusion imaging. Nat. Neurosci. 6, 750–757.

Burri, R., Bigler, P., Straehl, P., Posse, S., Colombo, J.P., Herschkowitz, N., 1990. Brain development: 1H magnetic resonance spectroscopy of rat brain extracts compared with chromatographic methods. Neurochem. Res. 15 (10), 1009–1016.

Catani, M., Jones, D.K., ffytche, D.H., 2005. Perisylvian language networks of the human brain. Ann. Neurol. 57 (1), 8–16.

Conturo, T.E., Lori, N.F., Cull, T.S., Akbudak, E., Snyder, A.Z., Shimony, J.S., McKinstry, R.C., Burton, H., Raichle, M.E., 1999. Tracking neuronal fiber pathways in the living human brain. Proc. Natl. Acad. Sci. U. S. A. 96 (18), 10422–10427.

Dejerine, J., 1895. Anatomie des Centres Nerveux. Rueff et Cie, Paris.

Duvernoy, H.M., 1999. The Human Brain Surface, Blood Supply and Three-Dimensional Sectional Anatomy. Springer-Verlag, Wein, NY.

Ellegood, J., Hanstock, C., Beaulieu, C., 2005a. Diffusion tensor spectroscopy (DTS) of human brain. Proc 13th Annual Meeting, ISMRM, 2005, Miami.

Ellegood, J., Hanstock, C.C., Beaulieu, C., 2005b. Trace apparent diffusion coefficients of metabolites in human brain using diffusion weighted magnetic resonance spectroscopy. Magn. Reson. Med. 53 (5), 1025–1032.

Ellegood, J., Hanstock, C.C., Beaulieu, C., 2006. Diffusion tensor spectroscopy (DTS) of human brain. Magn. Reson. Med. 55 (1), 1–8.

Falzi, G., Perrone, P., Vignolo, L.A., 1982. Right–left asymmetry in anterior speech region. Arch. Neurol. 39 (4), 239–240.

Foundas, A.L., Leonard, C.M., Heilman, K.M., 1995. Morphologic cerebral asymmetries and handedness. The pars triangularis and planum temporale. Arch. Neurol. 52 (5), 501–508.

Galaburda, A.M., LeMay, M., Kemper, T.L., Geschwind, N., 1978a. Right-left asymmetrics in the brain. Science 199 (4331), 852–856.

Galaburda, A.M., Sanides, F., Geschwind, N., 1978b. Human brain. Cytoarchitectonic left-right asymmetries in the temporal speech region. Arch. Neurol. 35 (12), 812–817.

Galaburda, A.M., Corsiglia, J., Rosen, G.D., Sherman, G.F., 1987. Planum temporale asymmetry, reappraisal since Geschwind and Levitsky. Neuropsychologia 25, 853–868.

Galuske, R.A., Schlote, W., Bratzke, H., Singer, W., 2000. Interhemispheric asymmetries of the modular structure in human temporal cortex. Science 289 (5486), 1946–1949.

Gannon, P.J., Holloway, R.L., Broadfield, D.C., Braun, A.R., 1998. Asymmetry of chimpanzee planum temporale: humanlike pattern of Wernicke's brain language area homolog. Science 279 (5348), 220–222.

Geschwind, N., Levitsky, W., 1968. Human brain: left–right asymmetries in temporal speech region. Science 161 (837), 186–187.

Harada, M., Uno, M., Hong, F., Hisaoka, S., Nishitani, H., Matsuda, T., 2002. Diffusion-weighted in vivo localized proton MR spectroscopy of human cerebral ischemia and tumor. NMR Biomed. 15 (1), 69–74.

Hopkins, W.D., Marino, L., Rilling, J.K., MacGregor, L.A., 1998. Planum temporale asymmetries in great apes as revealed by magnetic resonance imaging (MRI). NeuroReport 9 (12), 2913–2918.

Josse, G., Tzourio-Mazoyer, N., 2004. Hemispheric specialization for language. Brain Res. Brain Res. Rev. 44 (1), 1–12.

Jones, D.K., Simmons, A., Williams, S.C., Horsfield, M.A., 1999. Non-invasive assessment of axonal fiber connectivity in the human brain via diffusion MRI. Magn. Reson. Med. 1, 37–41.

Josse, G., Mazoyer, B., Crivello, F., Tzourio-Mazoyer, N., 2003. Left planum temporale: an anatomical marker of left hemispheric specialization for language comprehension. Brain Res. Cogn. Brain Res. 18 (1), 1–14.

Kroenke, C.D., Ackerman, J.J., Yablonskiy, D.A., 2004. On the nature of the NAA diffusion attenuated MR signal in the central nervous system. Magn. Reson. Med. 52 (5), 1052–1059.

Lamantia, A.S., Rakic, P., 1990. Cytological and quantitative characteristics of four cerebral commissures in the rhesus monkey. J. Comp. Neurol. 291 (4), 520–537.

Lehericy, S., Ducros, M., Krainik, A., Francois, C., Van de Moortele, P.F., Ugurbil, K., Kim, D.S., 2004. 3-D diffusion tensor axonal tracking shows distinct SMA and pre-SMA projections to the human striatum. Cereb. Cortex 14 (12), 1302–1309.

Lukas, J.R., Aigner, M., Denk, M., Heinzl, H., Burian, M., Mayr, R., 1998. Carbocyanine postmortem neuronal tracing. Influence of different parameters on tracing distance and combination with immunocytochemistry. J. Histochem. Cytochem. 46, 901–910.

Makris, N., Kennedy, D.N., McInerney, S., Sorensen, A.G., Wang, R., Caviness, V.S.J, Pandya, D.N., 2005. Segmentation of subcomponents within the superior longitudinal fascicle in humans: a quantitative, in vivo, DT-MRI study. Cereb. Cortex 15, 854–869.

Moffat, S.D., Hampson, E., Lee, D.H., 1998. Morphology of the planum temporale and corpus callosum in left handers with evidence of left and right hemisphere speech representation. Brain 121 (Pt 12), 2369–2379.

Mori, S., Crain, B.J., Chacko, V.P., van Zijl, P.C., 1999. Three-dimensional tracking of axonal projections in the brain by magnetic resonance imaging. Ann. Neurol. 45 (2), 265–269.

Nadler, J.V., Cooper, J.R., 1972. *N*-acetyl-L-aspartic acid content of human neural tumours and bovine peripheral nervous tissues. J. Neurochem. 19 (2), 313–319.

Nicolay, K., Braun, K.P., Graaf, R.A., Dijkhuizen, R.M., Kruiskamp, M.J., 2001. Diffusion NMR spectroscopy. NMR Biomed. 14 (2), 94–111.

Nucifora, P.G., Verma, R., Melhem, E.R., Gur, R.E., Gur, R.C., 2005. Leftward asymmetry in relative fiber density of the arcuate fasciculus. NeuroReport 16 (8), 791–794.

Parker, G.J., Haroon, H.A., Wheeler-Kingshott, C.A., 2003. A framework for a streamline-based probabilistic index of connectivity (PICo) using a structural interpretation of MRI diffusion measurements. J. Magn. Reson. Imaging 18 (2), 242–254.

Parker, G.J., Luzzi, S., Alexander, D.C., Wheeler-Kingshott, C.A., Ciccarelli, O., Lambon Ralph, M.A., 2005. Lateralization of ventral and dorsal auditory-language pathways in the human brain. NeuroImage 24 (3), 656–666.

Penhune, V.B., Zatorre, R.J., MacDonald, J.D., Evans, A.C., 1996. Interhemispheric anatomical differences in human primary auditory cortex: probabilistic mapping and volume measurement from magnetic resonance scans. Cereb. Cortex 6 (5), 661–672.

Posse, S., Cuenod, C.A., Le Bihan, D., 1993. Human brain: proton diffusion MR spectroscopy. Radiology 188 (3), 719–725.

Powell, H.W., Parker, G.J., Alexander, D.C., Symms, M.R., Boulby, P.A., Wheeler-Kingshott, C.A., Barker, G.J., Noppeney, U., Koepp, M.J., Duncan, J.S., 2006. Hemispheric asymmetries in language-related pathways: a combined functional MRI and tractography study. NeuroImage 32 (1), 388–399.

Song, S.K., Sun, S.W., Ramsbottom, M.J., Chang, C., Russell, J., Cross, A.H., 2002. Dysmyelination revealed through MRI as increased radial (but unchanged axial) diffusion of water. NeuroImage 17 (3), 1429–1436.

Song, S.K., Yoshino, J., Le, T.Q., Lin, S.J., Sun, S.W., Cross, A.H., Armstrong, R.C., 2005. Demyelination increases radial diffusivity in corpus callosum of mouse brain. NeuroImage 26 (1), 132–140.

Takahashi, M., Hackney, D.B., Zhang, G., Wehrli, S.L., Wright, A.C., O'Brien, W.T., Uematsu, H., Wehrli, F.W., Selzer, M.E., 2002. Magnetic resonance microimaging of intraaxonal water diffusion in live excised lamprey spinal cord. Proc. Natl. Acad. Sci. U. S. A. 99 (25), 16192–16196.

Upadhyay, J., Ducros, M., Knaus, T.A., Lindgren, K.A., Silver, A., Tager-Flusberg, H., Kim, D.S., 2006. Function and connectivity in human primary auditory cortex: a combined fMRI and DTI study at 3 Tesla. Cereb. Cortex 17 (10), 2420–2432.

Urenjak, J., Williams, S.R., Gadian, D.G., Noble, M., 1993. Proton nuclear magnetic resonance spectroscopy unambiguously identifies different neural cell types. J. Neurosci. 13 (3), 981–989.

Vernooij, M.W., Smits, M., Wielopolski, P.A., Houston, G.C., Krestin, G.P., van der Lugt, A., 2007. Fiber density asymmetry of the arcuate fasciculus in relation to functional hemispheric language lateralization in both right- and left-handed healthy subjects: a combined fMRI and DTI study. NeuroImage 35 (3), 1064–1076.

Zhai, G., Lin, W., Wilber, K.P., Gerig, G., Gilmore, J.H., 2003. Comparisons of regional white matter diffusion in healthy neonates and adults performed with a 3.0-T head-only MR imaging unit. Radiology 229 (3), 673–681.